

Low-Complexity Monitoring and Compensation of Transceiver IQ Imbalance by Multi-dimensional Architecture for Dual-Polarization 16 Quadrature Amplitude Modulation

YUKUN ZHANG,¹,XIAOXUE GONG,^{1,*},XU ZHANG² AND LEI GUO²

¹*School of Communications and Information Engineering, Chongqing University of Posts and Telecommunications, Chongqing 400065, China*

²*School of Computer Science and Engineering, Northeastern University, Shenyang 110167, China*

**Gongxx@cqupt.edu.cn*

Abstract: In this paper, a low-complexity IQ imbalance compensation architecture is proposed, which reduces the effects of in-phase (I) and quadrature (Q) imbalance. The architecture consists of transceiver IQ skew estimation methods and a low-complexity MIMO equalizer structure. Before the IQ skew estimation, the chromatic dispersion(CD) is pre-compensated in the transmitter(TX) by chirp filtering. The receiver(RX) IQ skew is estimated by Gardner's phase detector, and the TX skew is estimated by finding the value that yields the lowest equalizer error. The low-complexity MIMO equalizer consists of a complex-valued MIMO(CV-MIMO) and a real-valued DD-LMS MIMO(RV-MIMO), which employ a butterfly and a non-butterfly structure, respectively. The CV-MIMO is used to perform polarization demultiplexing. The RV-MIMO equalizes each of the two polarisations and simultaneously compensates for the TX IQ imbalance. The architecture first compensates for the IQ skew at low-complexity, and the other imperfections are compensated by the low-complexity MIMO equalizer. Therefore, this architecture can equalize signals impaired by the transceiver IQ imbalance with low complexity. A 100 km transmission simulation and experiment with 36 Gbaud dual-polarization quadrature amplitude modulation(DP-QAM) signals and offline DSP showed that, with the RX IQ skew estimation, the number of real multiplications is reduced by more than 70% compared with conventional cases. With the low-complexity MIMO equalizer, the number of real multiplications is reduced by 51% compared with 4×4 MIMO.

1. Introduction

To accommodate the increasing demand for data rate, passive optical network(PON) are transitioning to high symbol rates and high spectral efficiency modulation formats. High-order quadrature amplitude modulation (QAM) with a high baud rate has the potential to increase the data rate and efficiency. However, the QAM signal require more complex transceiver to send and receive it. For example, the dual-polarisation optical QAM signal must pass through a dual-polarization 90° optical hybrid, balanced photodetector(BPD) and transimpedance amplifier(TIA) to be demodulated. These components may impair the signal under unideal conditions. In an unideal condition, it is common to have a timing misalignment (IQ skew) of several picoseconds between the in-phase(I) and quadrature (Q)paths, or amplitude/phase imbalance between I and Q. Such as waveguide length mismatches between I/Q arms, TIA delay and gain imbalance, or any imperfection in the optical front-end. These imbalances are commonly calibrated during the manufacturing process. However, some residual imbalances can remain. In addition, environmental and mechanical factors, including temperature fluctuations and device aging, cause dynamic changes in IQ imperfection. At higher symbol rates, this post-calibration residual imbalance has a more severe impact than on lower symbol-rate transmissions. The technical document for the 400ZR coherent optical interface[30] stipulates that IQ skew should be less than 0.75 ps while IQ amplitude and phase imbalances must not exceed 1 dB and $\pm 5^\circ$

respectively. Thus, for high symbol-rate transmissions, an algorithm robust to IQ imbalance or a method to estimate the IQ imbalance is required.

Recently, some IQ imbalance-tolerant MIMO adaptive equalizers were proposed. References [1] propose equalizing to each in-phase and quadrature in each polarization, having four real-valued inputs and four real-valued outputs. This is a well-known real-valued 4×4 MIMO structure. References [2] propose independent chromatic dispersion (CD) compensation for each I and Q. After that, References [2] perform a 4×2 MIMO adaptive equalizer to compensate for IQ imbalance. References [3] propose an 8×2 MIMO adaptive equalizer structure. The new structure not only compensates for the IQ imbalance in single polarization but also for the presence of arbitrary crosstalk across four IQ lanes of polarization-multiplexed transceivers. References [4, 5] propose a complex-valued adaptive equalizer structure that can compensate for linear IQ-mixing effects at the receiver (RX) front end. References [6] proposed using the strictly linear and widely linear filters to compensate for the IQ imbalance over 10000 km. However, the conventional receiver IQ imbalance compensation methods based on the AEQ suffer from IQ skew-enhanced timing jitter incurred by the clock recovery algorithm [9]. In addition, imbalance-tolerant MIMO equalizers require more taps and multiple iterations, which introduces an increase in complexity. Therefore, skew-tolerant MIMO demands more area in practical ASIC implementations in comparison to common complex-valued 2×2 MIMO equalizers.

Therefore, some IQ skew monitor algorithms based on a clock recovery algorithm were proposed. References [7–9] use a digital Godard's phase detector (Godard's PD) to monitor the transceiver's IQ skew. References [10, 11] propose a robust receiver IQ skew monitoring scheme using a modified Godard's PD algorithm tailored for non-integer oversampling receivers. References [12–14] propose a receiver IQ skew monitoring scheme using a modified Gardner's phase detector (Gardner's PD) algorithm or an absolute phase detector algorithm. In general, Gardner's PD is better than Godard's PD because Gardner's PD doesn't require the extra FFT. However, the IQ skew monitor based on Gardner's PD algorithm is suitable only for short fiber transmission length due to fiber polarization mode dispersion (PMD) and chromatic dispersion (CD). When the signal polarization rotation (SOP) angle crosses 42.5° and the differential group delay (DGD) is $1/2$ symbol period [7, 8], the algorithms will fail in Gardner's PD algorithms [15]. The skew monitor using Gardner's PD is influenced by CD compensation, which will be studied in subsequent content. Some methods estimate the IQ imbalance based on data-aid. Reference [16] uses the concatenation of the pure real and imaginary sequences in the time domain to estimate the transceiver IQ skew. Reference [17] proposed a scheme based on cross-power-spectrum analysis for IQ imperfections. The proposed cross-power-spectrum scheme exhibits up to ± 200 ps for the skew of the coherent optical transceivers. To achieve wide-range IQ skew calibration simultaneously, Reference [18] studies propose utilizing the cross-correlation of time domain signals to extract delay information.

Because the IQ imbalance varies slowly, it is unnecessary to monitor it frequently. The current methods that compensate for the IQ imbalance are inefficient. For example, equalizers add more taps to compensate for receiver IQ imbalance. The methods that estimate the IQ imbalance based on data-aid need extra area in the circuit and increase the complexity. In addition, the IQ skew is the primary factor influencing the bit error rate (BER). Reference [19] clearly shows that the effective SNR reduction of the three factors is skew \gg amp. imbalance \gg pha. imbalance. Reference [20] shows that for a 100 GBaud 16QAM signal, the IQ skew should be less than 1.1 ps when the signal-to-noise ratio (SNR) penalty is less than 1 dB. Therefore, the IQ skew should first be extracted using low-hardware-resource methods, and then MIMO can reduce the number of taps to equalize signal. Skew monitoring based on Godard's PD is a low-hardware-resource method, but it needs FFTs.

In this paper, we introduce a low-complexity IQ imbalance compensation architecture for DP-16QAM in 100 km single-mode fiber (SSMF) transmission. First, the transceiver IQ skew

is estimated and compensated. We use Gardner's PD to estimate the receiver IQ skew. Due to the low PMD coefficient, the DGD over 100 km of SSMF does not approach half the symbol period. Therefore, Gardner's PD remains robust even when the SOP angle crosses 42.5° , since the required concurrent condition of $DGD = T/2$ is not satisfied. Rx IQ skew is added to a signal after accumulation of CD, but when CD compensation is performed first, the IQ impairments become mixed in a complicated way. Thus, we set the CD compensation in the transmitter(TX) DSP to avoid this problem. Moreover, for low complexity, we select the chirp filtering technique to compensate CD. Then, we configure a scanning method to estimate the TX IQ skew. The scanning method estimates and compensates the TX IQ skew by finding the value that yields the lowest equalizer error. Second, we designed a low-complexity equalizer to compensate for the TX amplitude and phase imbalance. We combine the complex-valued MIMO(CV-MIMO) and the real-valued MIMO(RV-MIMO) for signal equalization, which employ a butterfly and a non-butterfly structure, respectively. The CV-MIMO is used to perform polarization demultiplexing. The RV-MIMO equalizes each of the two polarisations and simultaneously compensates for the TX IQ imbalance. Since the TX and RX skew are being compensated, the new equalizer can equalize the signal with fewer taps. For convenience, the new equalizer is called C-R AEQ. The simulation results demonstrate that the RX skew estimation error is less than 0.2 ps, and the TX IQ skew estimation error is less than one-sixteenth of a symbol period. The residue TX IQ skew can be compensated by C-R AEQ. The C-R AEQ tolerates phase imbalance up to ± 10 degrees and amplitude imbalance up to ± 0.15 . Compared to the 4×4 MIMO equalizer, the C-R AEQ reduces the complexity by approximately half. In the experiment, we conducted 100 km SSMF transmissions following in-field calibration using the proposed method. The study utilized 36 GBaud 16 QAM signals to investigate the enhancement of Q-factor under different IQ balance conditions. The experimental results corroborate the simulation conclusion as well.

2. Working principle and simulations

2.1. Working principle

The signal can be expressed as $s(t) = s_I(t) + js_Q(t)$. Assuming that the signal $\hat{s}_1(t)$ is added IQ skew by a delay τ in receiver, which can be expressed as

$$\hat{s}_1(t) = s_I(t) * \delta\left(t - \frac{\tau}{2}\right) + js_Q(t) * \delta\left(t + \frac{\tau}{2}\right) \quad (1)$$

where the $*$ represents a convolution operation. Let $S(\omega) = \mathcal{F}\{\hat{s}_1(t)\}$, in frequency domain, the Eq.1 can be expressed as

$$S(\omega) = S_I(\omega)e^{-j\omega\tau/2} + jS_Q(\omega)e^{j\omega\tau/2} \quad (2)$$

Where the $S_I(\omega) = \mathcal{F}\{s_I(t)\}$, and $S_Q(\omega) = \mathcal{F}\{s_Q(t)\}$. According to Eq. 2, the delay τ introduces respective linear phases shift to $S_I(\omega)$ and $S_Q(\omega)$ in frequency domain. Therefore, the transmission matrix of delay τ in the frequency domain can be calculated by

$$H_\tau(\omega) = \begin{bmatrix} \frac{\text{real}(S(\omega))}{S_I(\omega)} & 0 \\ 0 & \frac{\text{imag}(S(\omega))}{S_Q(\omega)} \end{bmatrix} = \begin{bmatrix} e^{-j\omega\tau/2} & 0 \\ 0 & e^{j\omega\tau/2} \end{bmatrix} \quad (3)$$

In general, this delay cannot be corrected by the all-digital feedback clock recovery algorithm(CRA). The CRA completes the timing adjustment by calculating the fractional interval μ_k [21]. When the clock is recovered, the sample point will be adjusted to the optimum detection of the symbol, as shown in Fig. 1(a). However, if there are IQ skews in X polarization or Y polarization, the numerically controlled oscillator(NCO) outputs $\hat{\mu}_k$ leading to the error

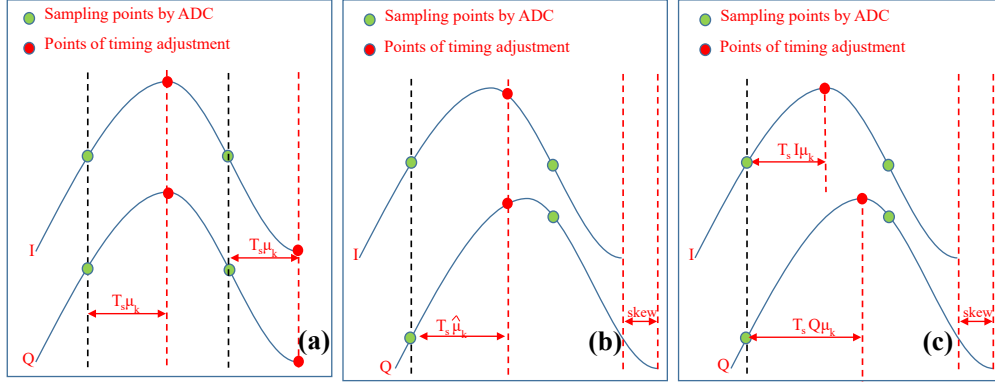


Fig. 1. (a)Clock recovery Without IQ skew(b)Clock recovery With IQ skew,(c)Principle of IQ skew monitoring by clock recovery

sampling instant, as shown in Fig. 1(b). So, if we calculate the I and Q μ_k separately, as shown in Fig.1(c), then we can calculate the value of IQ skew by

$$X_{IQskew} = \frac{1}{2\text{Baud}} \text{mean}(U_{XI} - U_{XQ}) \quad (4)$$

$$Y_{IQskew} = \frac{1}{2\text{Baud}} \text{mean}(U_{YI} - U_{YQ}) \quad (5)$$

Where X_{IQskew} , Y_{IQskew} are the receiver IQ skew of the X polarization and Y polarization(Pol), Baud is the symbol rate. 2Baud is the sample rate. The notation $\text{mean}()$ represents the average calculation. U_{XI} , U_{XQ} , U_{YI} , U_{YQ} are fractional intervals of I and Q in each Pol.

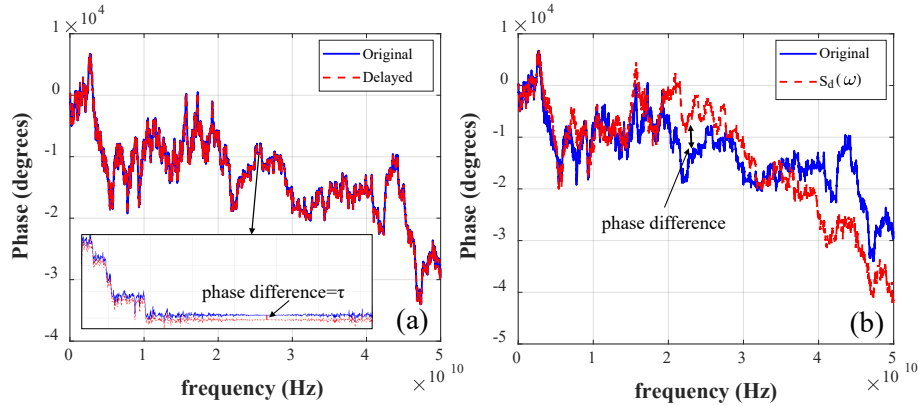


Fig. 2. (a)The phase difference between the original and delayed signal without CD compensation(b)The phase difference between the original and delayed signal with CD compensation

However, the CD compensation will affect the algorithm. If the fiber has a CD and the CD has been compensated in the receiver, the skew monitoring cannot calculate the receiver IQ skew. The reason is explained using the WL mode [4]. Let $h_{cd}(t) = \mathcal{F}^{-1}\{H_{cd}(\omega)\}$, we can write

$h_{cd}(t) = h_{cd,I}(t) + jh_{cd,Q}(t)$. Thus, the $\hat{s}(t)$, which suffers from CD and receiver IQ skew, can be represented by:

$$\begin{bmatrix} \hat{s}_I(t) \\ \hat{s}_Q(t) \end{bmatrix} = \begin{bmatrix} h_{cd,I}(t) & -h_{cd,Q}(t) \\ h_{cd,Q}(t) & h_{cd,I}(t) \end{bmatrix} \begin{bmatrix} \delta(t - \frac{\tau}{2}) & 0 \\ 0 & \delta(t + \frac{\tau}{2}) \end{bmatrix} \begin{bmatrix} s_I(t) \\ s_Q(t) \end{bmatrix} \quad (6)$$

Therefore, $\hat{s}(t)$ can be expressed as:

$$\hat{s}(t) = h_1(t) * s(t) + h_2(t) * s^*(t) \quad (7)$$

$$h_1(t) = \frac{1}{2} \left\{ \begin{array}{l} h_{cd,I}(t - \frac{\tau}{2}) + h_{cd,I}(t + \frac{\tau}{2}) \\ + j \left[h_{cd,Q}(t + \frac{\tau}{2}) + h_{cd,Q}(t - \frac{\tau}{2}) \right] \end{array} \right\} \quad (8)$$

$$h_2(t) = \frac{1}{2} \left\{ \begin{array}{l} h_{cd,I}(t - \frac{\tau}{2}) - h_{cd,I}(t + \frac{\tau}{2}) \\ + j \left[h_{cd,Q}(t + \frac{\tau}{2}) - h_{cd,Q}(t - \frac{\tau}{2}) \right] \end{array} \right\} \quad (9)$$

Where $H_{cd}(\omega)$ is the frequency response of the CD. $(.)^*$ denotes the complex conjugate operation. let $\hat{S}(\omega) = \mathcal{F}\{\hat{s}(t)\}$, $S(\omega) = \mathcal{F}\{s(t)\}$. Using $H_{cd}^{-1}(\omega)$ compensate $\hat{S}(\omega)$, the result is:

$$H_{cd}(\omega) = e^{-j(\beta_2\omega_c)/2\omega^2L} \quad (10)$$

$$\begin{aligned} S_d(\omega) &= H_{cd}^{-1}(\omega)\hat{S}(\omega) \\ &= \cos\left(\frac{\omega\tau}{2}\right)S(\omega) - j[H_{cd}^*(\omega)]^2 \sin\left(\frac{\omega\tau}{2}\right)S^*(-\omega) \end{aligned} \quad (11)$$

Where $S_d(\omega)$ is the signal after CD compensation in the frequency domain. Skew monitoring requires extracting the phase shift τ from $\hat{s}_1(t)$. The frequency domain of $\hat{s}_1(t)$ correspond to $S(\omega) = H_\tau(\omega) \begin{bmatrix} S_I(\omega) \\ S_Q(\omega) \end{bmatrix}$. However, from Eq.11, Eq.2, and Eq.3, it can be found that the $H_\tau(\omega)$ can not be derived from $S_d(\omega)$. Because $S_d(\omega)$ contains a component which consists of the complex conjugate of the $S(\omega)$. In other words, if $\tau \neq 0$, according to Eq.11, the $S(\omega) \neq S_d(\omega)$. Therefore, the receiver IQ skew cannot be detected when the CD is compensated in the receiver. Fig.2 shows this difference. Fig.2(a) shows the phase shift between the delayed signal and the original signal in the frequency domain. It is observed in Fig.2(a) that the delayed signal always keeps a fixed phase difference between the delayed signal and the original signal. This means that the delay τ can be detected by the skew monitoring. Fig.2(b) shows the phase shift between the $S_d(\omega)$ and the original signal in the frequency domain. It is observed in Fig.2(b) that the phase difference changes when the ω changes. According to Eq.3, the delay τ cannot be detected by the skew monitoring.

To further illustrate the CD compensation and IQ skew interaction at the receiver. Fig.3(a) is the skew monitoring, which is set at the receiver. The TED is Gardner's PD. X_i , X_q , Y_i , and Y_q are the I and Q of X polarization and Y polarization, respectively. The skew calculation module is composed of four CRA. X_i , X_q , Y_i , and Y_q input the four CRA, respectively, and each CRA outputs a fractional interval to obtain the U_{X_I} , U_{X_Q} , U_{Y_I} , U_{Y_Q} , then, the IQ skew for the corresponding polarization is obtained using Eq.4 and Eq.5. The CD compensation is set before skew monitoring. In Fig. 3(b), the estimation results are plotted as a function of fiber length, for a CD coefficient $= -16 \text{ ps}/(\text{nm} \cdot \text{km})$ in fiber. It should be noted that the skew monitoring runs after CD compensation is completed when the transmission length is greater than 10 km. And the transmission length is less than 10 km, the CD compensation is not performed. The RX IQ skew is set to 3.9 ps in the receiver. After the CD compensation is complete, the skew calculation

pol equalize error $M(e(n)_y)_{\tau_y}$ after each performs Eq.17 and Eq. 18, which can be expressed as

$$M(e(n)_x)_{\tau_x} = \sum_{n=1}^N \frac{e(n)_x}{N} \quad (19)$$

$$M(e(n)_y)_{\tau_y} = \sum_{n=1}^N \frac{e(n)_y}{N} \quad (20)$$

Where N is the number of symbols. Then the X pol and Y pol $M(e(n))$ are sent to the scan controller. It should be noted that the τ_x and τ_y are respective scanning from $-3/16T$ to $3/16T$, the scan controller stores a number of $M(e(n)_x)_{\tau_x}$ ($\tau_x=(-3T/16, -2T/16...2T/16,3T/16)$) and $M(e(n)_y)_{\tau_y}$ ($\tau_y=(-3T/16, -2T/16...2T/16,3T/16)$). The scan controller selects the minimum $M(e(n)_x)_{\tau_x}$ and $M(e(n)_y)_{\tau_y}$. Then, the τ_x and τ_y are the rough skew estimation, and the rough TX IQ skew compensation module uses τ_x and τ_y to compensate for the TX IQ skew. The RX skew monitor is shown in Fig. 3(a).

To fine-compensate for the TX IQ skew, inspired by KM AEQ [23], we design a C-R AEQ, which is composed of complex-valued MIMO(CV-MIMO) and real-valued decision-directed least-mean-square (RV-DD-LMS). The CV-MIMO is composed of a butterfly structure with 6 taps per filter. The RV-DD-LMS is a non-butterfly filter for each of two polarizations after the FOE/CPE. Because we found that the FOE/CPE can be correctly performed after the signal is equalised by only a 3-tap CV-MIMO. The CV-MIMO is used for polarisation demultiplexing and to ensure the FOE/CPE can be correctly performed, and the RV-DD-LMS compensates the TX IQ imbalance and equalises each of the two polarisations. The tap coefficient vector of the RV-DD-LMS is updated according to reference [1]. C-R AEQ is similar to reference [24]. The difference is that the reference [24] does not consider CD and frequency offset. This means reference [24] is only suitable for self-homodyne coherent optical system in short transmission length.

2.2. Simulation

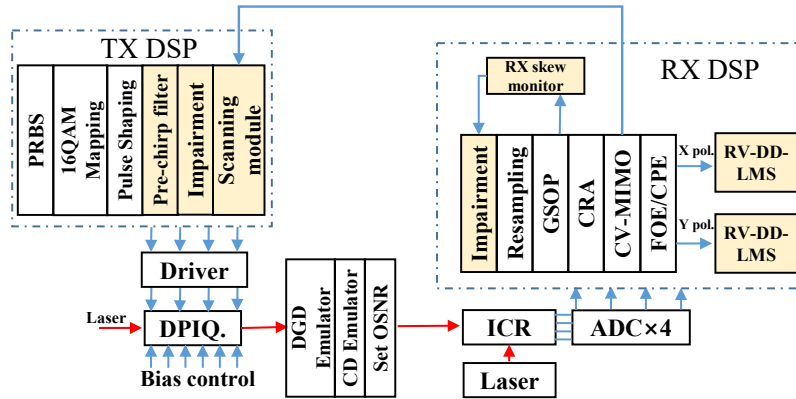


Fig. 6. System setup for 36 GBaud 16QAM

To confirm our proposed methods, a 36 Gbaud dual-polarization Nyquist 16QAM (DP-Nyquist-16QAM) signal with the system diagram displayed in Fig.6. In the transmitter, the full raised cosine filter is used to implement the pulse shape, and the roll-off factor is set to 0.5. The samples per symbol (SPS) are 4, and the pre-chirp filter block size is 264. Transmit a total of 2^{16} symbols. The TX skew is set from -6 ps to 6 ps (from $-T/4$ to $T/4$ of 36 Gbaud). The scanning module

scans in steps of $T/16$. We analyze the impact of polarization effects by the higher-order PMD model. The mean DGD is set to $0.5 \text{ ps/km}^{1/2}$ in the DGD emulator. The CD coefficient is $-16 \text{ ps}/(\text{nm} \cdot \text{km})$ in the CD emulator. The transmission length is 100 km. The OSNR is defined assuming a bandwidth of 12.5 GHz and is set to 23 dB. In the receiver, the RX skew is set from -6 ps to 6 ps (from $-T/4$ to $T/4T$ of 36 Gbaud). The signal is down-sampled to 2 SPS. The CV-MIMO tap numbers are set to 5 taps. The RV-DD-LMS tap number is set to 21 taps. The transceiver imbalances are digitally added in the DSP model of Rx and Tx. The transmission laser and the LO laser are operating at 1552.5 nm with a 100kHz linewidth and a 1 GHz frequency offset.

2.2.1. The Effect of pre-CD compensation on RX IQ Skew Estimation

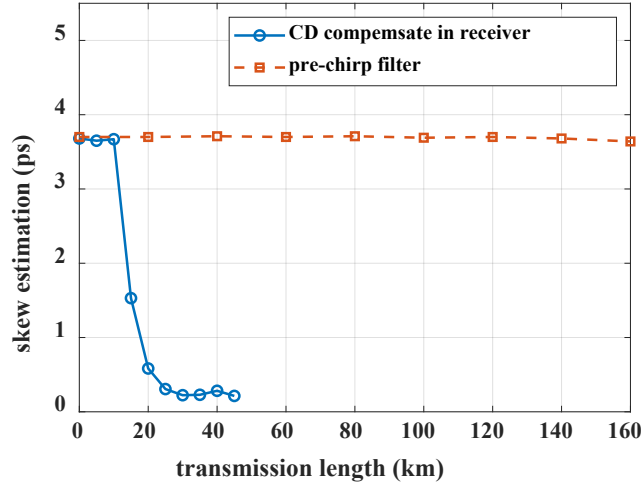


Fig. 7. The Effect of pre-CD compensation on RX IQ Skew Estimation

First, the relation between the location of the CD compensation and the RX IQ skew estimation is tested in simulation. To clearly observe the relationship, the RX X pol IQ skew is set at 3.9 ps, and other values of transceiver IQ imbalance are set to zero in this part. We use the pre-chirp filter in the transmitter or the FDE technique in the receiver to compensate for CD. The RX skew estimation is shown in Fig. 7. According to 7, it can be found that if the CD compensation is in the receiver, the RX IQ skew estimation is close to 0 ps when the transmitter length is larger than 20 km. But if the CD compensation is in the transmitter, the RX IQ skew estimation is close to 3.9 ps, and the result is unaffected by the transmission length. This simulation result demonstrates our proposed theory that the location of CD compensation is related to RX skew estimation, and the RX IQ skew can be detected after pre-CD compensation.

2.2.2. The Effect of Transceiver IQ Imbalance on RX IQ Skew Estimation

Next, the effect of the transceiver IQ imbalance on the RX IQ skew estimation is simulated. The RX X pol skew is set from -6 ps to 6 ps. In order to comprehensively observe the imperfect factor influence on the RX X pol skew estimation error, we consider the RX X pol amplitude imbalance, phase imbalance, RX Y pol skew, and TX X pol amplitude imbalance, phase imbalance, TX X pol skew. These results are shown via 2-Dimensional(2D) planes or 3-Dimensional(3D) surfaces. Unless otherwise stated, the basic IQ imbalance is X pol IQ imbalance. For example, RX skew is RX X pol skew, TX amplitude imbalance is TX X pol amplitude imbalance, RX skew estimation error is RX X pol skew estimation error, and so on. The Tx and RX amplitude imbalance varies

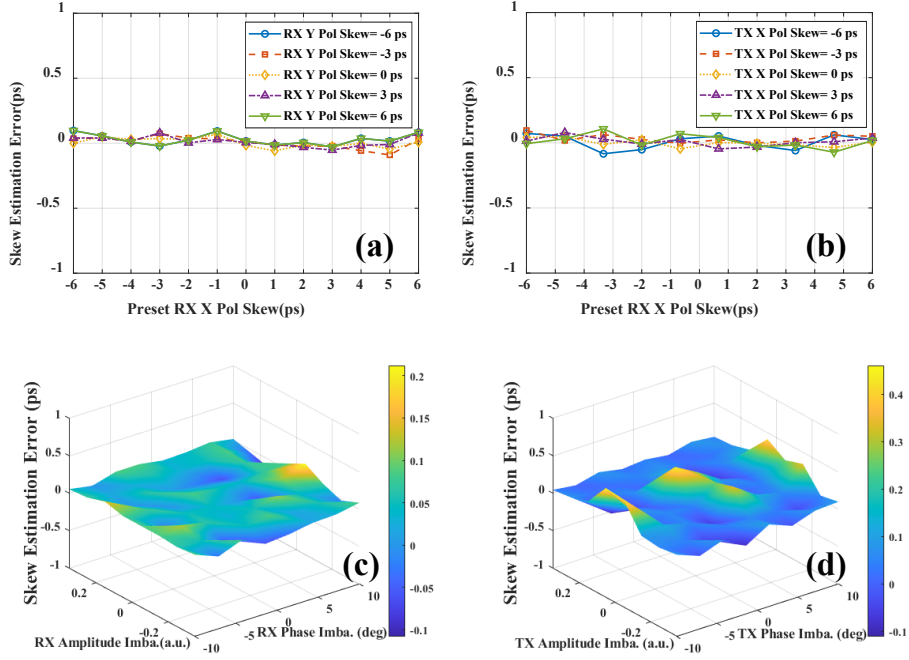


Fig. 8. (a)The relation between skew estimate error and RX X/Y pol IQ skew (b)The relation between skew estimate error and TX X pol IQ skew(c) The relation between skew estimate error and RX pmp./pha. imbalance(d) The relation between skew estimate error and TX pmp./pha. imbalance

from -0.35 to 0.35. The TX and RX phase imbalance varies from -10 degrees to 10 degrees. The TX skew and RX Y pol skew varies from -6 ps to 6 ps, and the RX skew changes from -6 ps to 6 ps. Based on these conditions, the RX skew estimation error is shown in Fig.8. The Fig.8(a) displays the relation between RX skew estimation and RX Y pol skew. As the RX Y pol skew changes -6 ps to 6 ps, the RX skew estimation error is always kept less than 0.3 ps. This means that the RX skew estimation is unaffected by RX Y pol skew. The Fig.8(b) displays the relation between RX skew estimation and TX skew. Due to the frequency offset isolate TX skew and RX skew[7], as the TX skew changes -6 ps to 6 ps, the RX skew estimation error is always kept less than 0.3 ps. This means that the RX skew estimation is unaffected by TX skew. The reason is that the frequency offset and phase noise isolate the TX imbalance. The Fig.8(c) displays the relation between RX skew estimation, RX amplitude imbalance, and RX phase imbalance. According to Fig.8(c), the RX skew estimation error is kept less than 0.3 ps when the amplitude imbalance changes from -0.35 to 0.35, and the phase imbalance varies from -10 degrees to 10 degrees. The Fig.8(d) displays the relation between RX skew estimation, TX amplitude imbalance, and TX phase imbalance. According to Fig.8(d), the RX skew estimation error is kept less than 0.5 ps when the amplitude imbalance changes from -0.35 to 0.35, and the phase imbalance varies from -10 degrees to 10 degrees. Therefore, according to Fig.8(a) - Fig.8(d), it can be concluded that the RX skew estimation is unaffected by transceiver IQ imbalance.

2.2.3. The Effect of Transceiver IQ Imbalance and OSNR on Rough TX IQ Skew Estimation

The rough TX IQ skew estimation is via error output by CV-MIMO. However, the error is affected by many factors, such as IQ imbalance, OSNR, and so on. We mainly consider the effect of transceiver IQ imbalance and OSNR on rough TX IQ skew estimation. The OSNR is set to 13

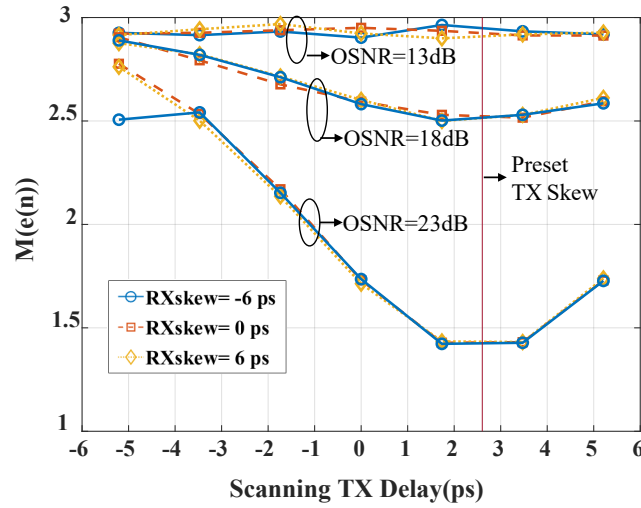


Fig. 9. $M(e(n))$ result varies with the OSNR and RX skew change

dB, 18 dB, and 23 dB, respectively. The TX skew is fixed as 2.6 ps ($1.5T/16$ of 36 GBaud), and the scanning module scans the TX delay at $T/16$ intervals. The Tx and RX amplitude imbalance varies from -0.35 to 0.35. The TX and RX phase imbalance varies from -10 degrees to 10 degrees. The RX skew is set to -6 ps, 0 ps, and 6 ps, respectively. The TX Y pol skew varies from -6 ps to 6 ps. Fig.9 displays the relation between OSNR and rough TX IQ skew estimation. First, we can find that when the OSNR is fixed, the $M(e(n))$ is unaffected by RX skew. Second, at OSNRs of 18 dB and 23 dB, $M(e(n))$ is minimum at 1.74 ps ($T/16$ of 36 GBaud) or 3.47 ps ($2T/16$ of 36 GBaud). From the scan control rule, the rough TX skew estimation is 1.74 ps or 3.47 ps. This means the residual TX skew is less than $T/16$ of 36 GBaud after rough TX skew compensation. However, if the OSNR is lower, such as 13 dB, the $M(e(n))$ can not display the correct rough TX skew estimation. The reason is that the noise is the main influence on $M(e(n))$ instead of TX skew. Fig.10 displays the effect of transceiver IQ imbalance on Rough TX IQ Skew Estimation. Fig.10(a) displays the relation between TX amplitude and phase imbalance and rough TX skew estimation error. Fig.10(b) displays the relation between RX amplitude and phase imbalance and rough TX skew estimation error. Fig.10(a) and Fig.10(b) display that the estimation error is kept less than ± 1 ps when the TX and RX phase and amplitude imbalance are changed. Fig.10(c) displays the relation between TX Y pol skew and rough TX Skew estimation error. Fig.10(c) displays that the estimation error is kept less than ± 1 ps when TX Y pol skew changes from -6 ps to 6 ps. According to Fig.10, it is concluded that the rough TX skew estimation error is unaffected by transceiver IQ imbalance, but is affected by the lower OSNR.

It should be noted that transmitted X pol can be received as X or Y pol and vice versa. Therefore, does not allow simultaneous scanning delay on X pol and Y pol. The reason is that the scan controller is difficult to distinguish which is the X pol $M(e(n))$ and which is the Y pol $M(e(n))$, because the X pol $M(e(n))$ and Y pol $M(e(n))$ change simultaneously.

2.2.4. Performance with Transmitter IQ Imbalance

In this part, we assess the performance of our proposed scheme under the transmitter IQ imbalance condition. Firstly, we assess the performance of C-R AEQ in transmitter IQ imbalance. The Tx amplitude imbalance varies from -0.35 to 0.35. The TX phase imbalance varies from -10 degrees to 10 degrees. The TX skew and TX Y pol skew vary from -6 ps to 6 ps. The Q-factor is used to display the signal quality after C-R AEQ. In order to clearly observe which is the major

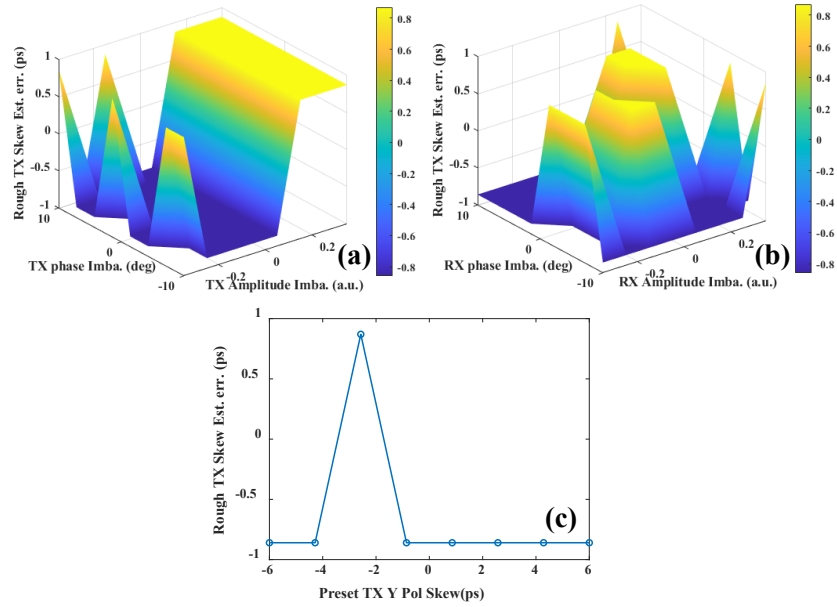


Fig. 10. (a) Rough TX skew estimation error with TX amp./pha. imbalance changing (b) Rough TX skew estimation error with RX amp./pha. imbalance changing (c) Rough TX skew estimation error with TX Y pol change

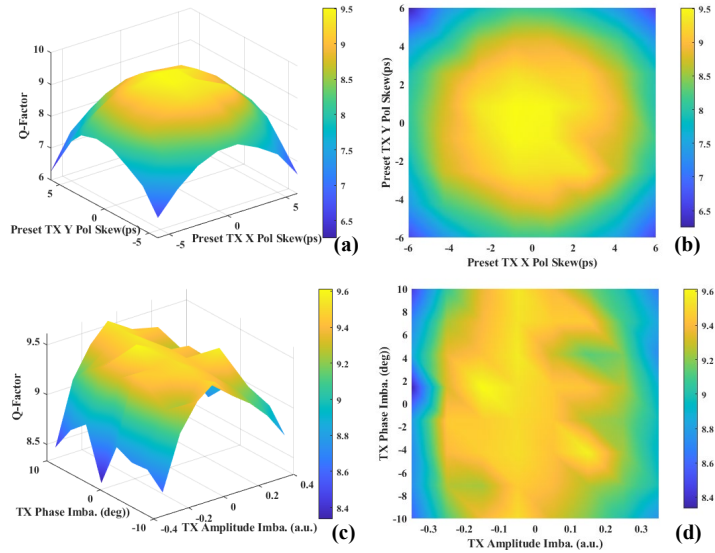


Fig. 11. (a) TX skew tolerance of the proposed architecture after 100 km transmission (b) Project the 3D surface of (a) on TX X pol skew and TX Y pol skew (c) TX amp./pha. imbalance tolerance of the C-R AEQ after 100 km transmission (d) Project the 3D surface of (c) on TX amp. imbalance and TX pha. imbalance

factor influencing the Q-factor, we study not only the 3D surfaces but also their 2D projections.

Fig.11(a) displays the TX skew tolerance of C-R AEQ, and Fig.11(b) is the 2D projections of Fig.11(a). According to Fig.11(a), the maximum Q is 9.5 dB when TX skew and TX Y pol skew are 0 ps. In addition, as the TX skew approaches ± 6 ps when the TX Y pol skew approaches ± 6 ps, the Q-factor is reduced to 6.3. This means that the TX skew is one of the major influences on the Q-factor. According to Fig.11(b), the Q penalty is 0.15 dB when the Tx skew and TX Y pol skew are less than ± 2 ps ($\pm 1/16$ of symbol period). From Fig.9 and Fig.10, the scanning module makes the residual TX skew less than 1 ps. Therefore, the C-R AEQ could compensate for the residual TX skew (fine TX skew compensation) after rough TX skew compensation. Fig.11(c) shows the TX amplitude and phase imbalance tolerance of C-R AEQ, and Fig.11(d) is the 2D projections of Fig.11(c). Seen from Fig.11(c), compare to Fig.11(a), TX amplitude and phase imbalance influence on Q-factor is lower than TX skew. The Q-factor is 0.84 when the TX amplitude approaches ± 0.35 , and the TX phase approaches ± 10 degrees. As shown in Fig.11(d), when the TX phase imbalance approaches ± 10 degrees, and there is no TX amplitude imbalance, the Q-factor remains 9.5 dB. In addition, when the TX amplitude imbalance changes from 0 to ± 0.35 , the Q-factor changes from 9.5 to 8.4 dB. This means that the TX phase imbalance has the least influence on Q-factor after C-R AEQ, whereas the amplitude imbalance has a greater influence on Q-factor than the phase imbalance.

2.2.5. Performance with Receiver IQ Imbalance

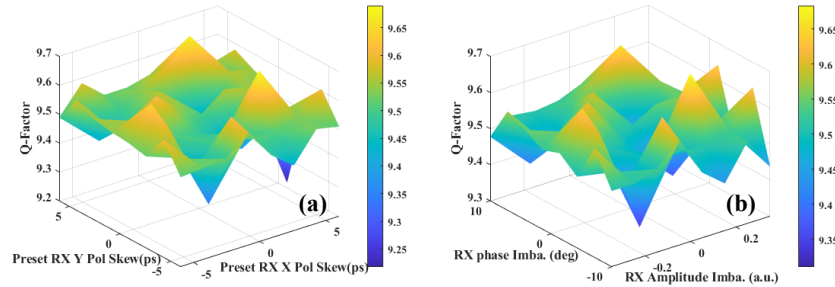


Fig. 12. (a)RX skew tolerance of proposed architecture after 100 km transmission(b)RX amp./pha. imbalance tolerance of proposed architecture after 100 km transmission

In this part, we assess the performance of our proposed scheme under the receiver IQ imbalance condition. The Rx amplitude imbalance varies from -0.35 to 0.35. The RX phase imbalance varies from -10 degrees to 10 degrees. The RX skew and RX Y pol skew vary from -6 ps to 6 ps. Fig.12(a) and Fig.12(b) display the Q-factor performance with RX skew, Y pol skew, RX phase, and amplitude imbalance. From Fig.12(a) and Fig.12(b), the maximum Q-factor is greater than 9.65 dB, and the minimum Q-factor is greater than 9.25 dB. Therefore, due to the GSOP and RX skew monitor, the Q-factor is unaffected by the RX IQ imbalance.

2.2.6. Performance with Transceiver IQ Imbalance

In real conditions, the IQ imbalance is present in both the transmitter and the receiver. In addition, we want to study performance under different OSNR conditions. To simulate that condition, the TX X/Y pol skew is set to 1 ps, since the scanning module makes the TX skew less than 1 ps. The TX X/Y pol amplitude imbalance is set to 0.1. The TX X/Y pol phase imbalance is set to 5 degrees. The RX X/Y pol skew is set to 3 ps. The RX X/Y pol amplitude imbalance is set to 0.1. The RX X/Y pol phase imbalance is set to 5 degrees. These imbalanced values are from reference [17] and our experimental results. The OSNR changes from 17 dB to 23 dB. For

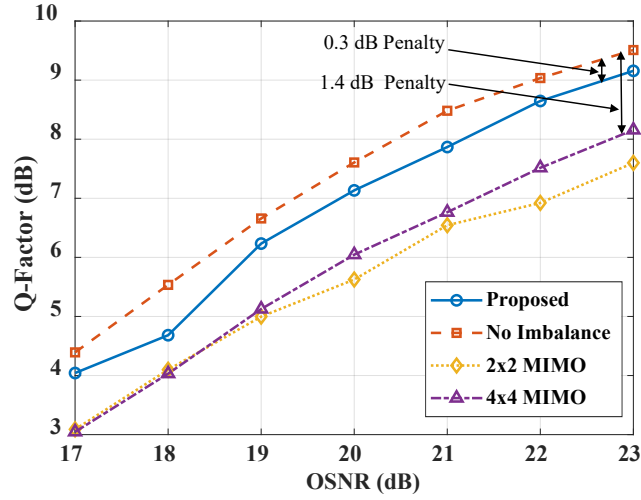


Fig. 13. Performance of proposed architecture with TX/RX X/Y pol imbalance after 100 km transmission

performance comparison, we use the perfectly balanced transceiver as the reference. To clearly observe the performance of our proposed methods, the 2×2, 4×4 MIMO with 33 taps per filter and our proposed methods are used to equalize the signal, meanwhile. The result is shown in Fig. 13, the Q-factor changes from 4.39 to 9.5 dB as the OSNR varies from 17 to 23 dB when there are no imbalances. The Q-factor changes from 4 to 9.2 dB as the OSNR varies from 17 to 23 dB via our proposed methods. The Q penalty is 0.3 dB when the OSNR changes from 19 dB to 23 dB. For comparison, the 2×2, 4×4 MIMO Q-factor changes from 3.1 to 7.6 dB and from 3 to 8.1 dB, respectively. The Q penalty is 1.4 dB when the 4×4 MIMO is used at an OSNR of 23 dB. This means that our proposed methods can reduce the Q penalty caused by transceiver IQ imbalance. Comparing our proposed methods with the 4×4 MIMO structure, we observe that the Q factor rises by more than 1 dB at an OSNR of 23 dB.

2.2.7. Performance with DGD after C-R AEQ

Since the butterfly structure has only 5 taps per filter in C-R AEQ, it is necessary to study the performance of PMD compensation. We set the polarization rotation angle to 45 degrees, and the DGD changes from 0 to 9 ps. The DGD values refer to reference [23]. Any IQ imbalance is set to zero in this part. For comparison, the 4×4 MIMO with 33 taps per filter and the proposed methods are used to equalize the signal, meanwhile. The result is shown in Fig. 14. It can be found that the proposed method is unaffected by DGD values ranging from 0 ps to 9 ps. In addition, the Q-factor after C-R AEQ is greater than the Q-factor after 4×4 MIMO by about 0.3 dB in the same DGD value. We think the reason is that the C-R AEQ further reduces the phase noise effect after CPR.

3. Experiment

We investigate the performance of the proposed scheme through experiments. The experimental setup is shown in Fig. 15. Two DFB lasers with a linewidth <100 kHz and a wavelength = 1551.12 nm are used as the signal carrier and local oscillator, respectively. A 92 GSa/s arbitrary waveform generator (AWG, Keysight M8196A) is used to generate the four tributaries of the 36 GBaud DP-Nyquist-16QAM signal with a ROF = 0.5, and the signal is resampled to 2.5 SPS.

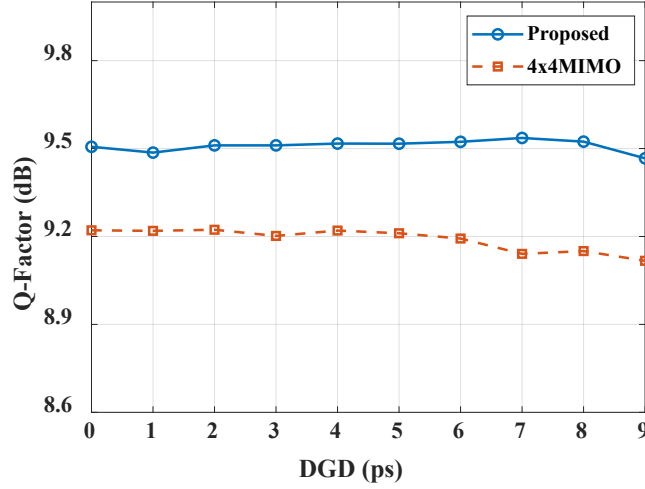


Fig. 14. Result of simulated DGD tolerance test

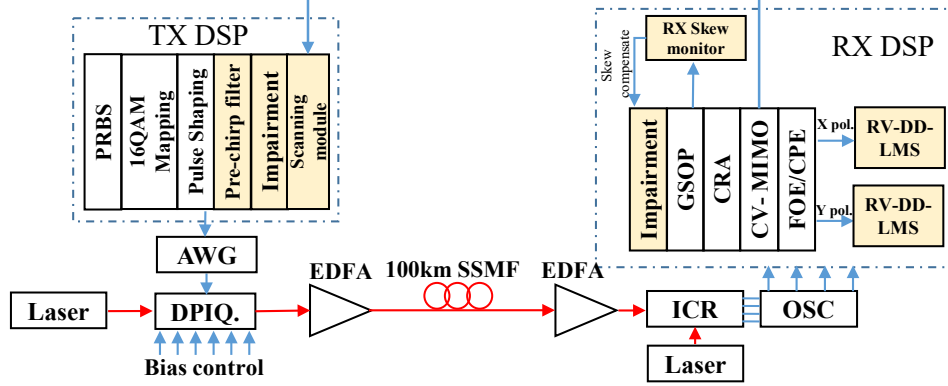


Fig. 15. The experimental setup and DSP flow diagram

Then modulated onto the optical carrier using a dual-polarization optical IQ modulator(DPIQ, FTM7977) with a 3-dB bandwidth of 23 GHz. The optical signal is amplified by two EDFAs and transmitted over a 100-km standard single-mode fiber(SSMF). At the receiver side, the optical signal is demodulated by an integrated coherent receiver (ICR, CPRV1225A) with a 3-dB bandwidth of 25 GHz. Finally, the signal was sampled by an oscilloscope (OSC, DSOZ594A) at a sample rate of 80 GHz. In TX DSP, the CD is compensated by a pre-chirp filter with a block size of 112, and the TX IQ imbalance is added digitally. In RX DSP, the signal is resampled to 2 SPS, and the RX IQ imbalance is added digitally first. The signal is input to the CRA after the Gram-Schmidt orthogonalization procedure (GSOP). Meanwhile, the signal is input to the RX skew monitor to calculate the RX skew. In Fig. 15, we set the receiver's X polarization(RX X pol.) IQ skew and Y polarization (RX Y pol.) IQ skew at 6 ps respectively. To verify the performance of our proposed methods, the experiments were repeated several times.

Fig. 16 displays the performance of our proposed methods with the receiver IQ imperfect. The Fig. 16(a) shows the accuracy of the receiver IQ skew estimation. In Fig. 16(a), the skew estimation is performed twenty times. According to Fig. 16(a), most skew calculation results are

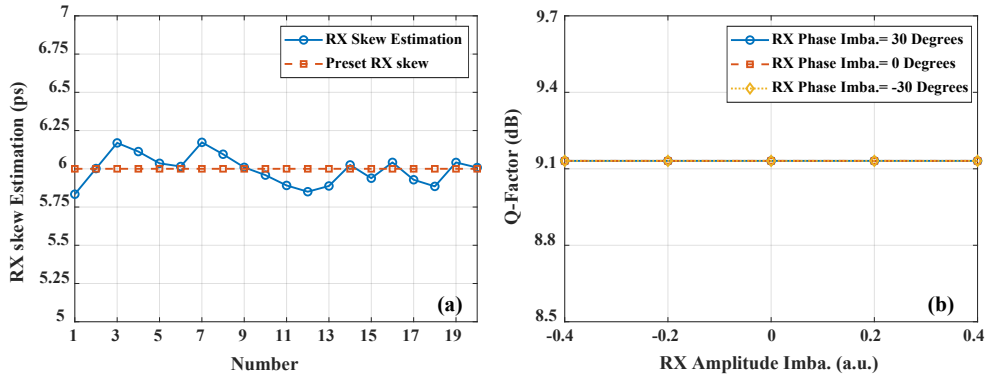


Fig. 16. (a)RX skew estimation after 20 times test(b)RX amp./pha. imbalance tolerance of the proposed architecture after 100 km transmission

around 6 ps, with a minimum of 5.8 ps and a maximum of 6.2 ps. This means our proposed scheme is effective and the estimation error is within ± 0.2 ps. The Fig. 16(b) displays the relation between Q-factor and receiver IQ amp./pha. imbalance after receiver IQ skew compensation. According to Fig. 16(b), the Q-factor is unaffected by IQ amp./pha. imbalance due to the GSOP.

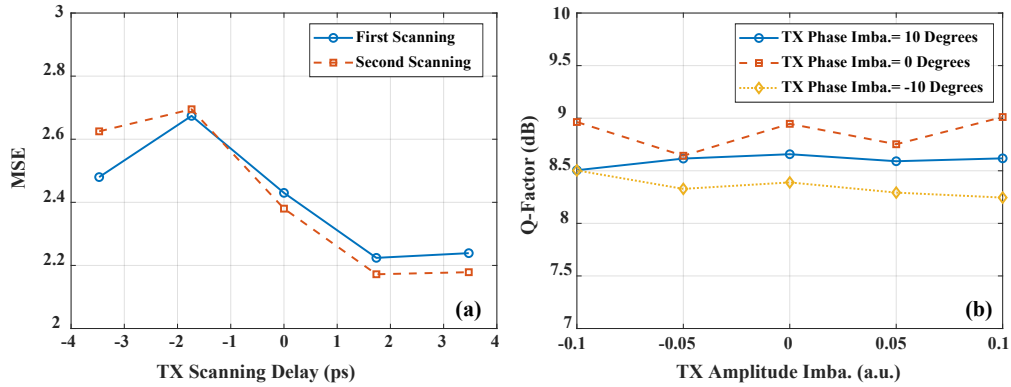


Fig. 17. (a)Rough TX skew estimation after 2 times scanning(b)TX amp./pha. imbalance tolerance of the proposed architecture after 100 km transmission

Fig. 17 displays the performance of our proposed methods with the transmitter IQ imperfect after RX X/Y pol skew compensation. The Fig. 17(a) shows the scanning module scans the TX delay result. In Fig. 17(a), the TX delay scans vary from $-2T/16$ to $2T/16$, and the MSEs are plotted as a function of TX delay. The TX Y pol skew is set to about 2.5 ps. The TX X pol skew is set to about 3.5 ps. The scanning delay is completely performed twice, which is the first scanning and the second scanning. According to The Fig. 17(a), the MSE is lowest when the TX scanning delay is 1.74 ps, both at the first and second scanning. Thus, the rough TX skew estimation is 1.74 ps. In Fig. 17(b), the TX amp./pha. imbalance is studied. The TX X/Y pol amplitude changes from -0.1 to 0.1, and the phase imbalance is respectively set to -10, 0, and 10 degrees. According to Fig. 17(b), the Q-factor remains stable when the amplitude imbalance varies from -0.1 to 0.1 with the phase imbalance fixed. On the other hand, the highest mean Q-factor is 8.7 dB when the TX phase imbalance is 0 degrees, and the lowest mean Q-factor is 8.3 dB when the TX phase imbalance is -10 degrees. This means that the Q penalty is 0.4 dB

when using our proposed methods in the phase imbalance range of -10 to 10 degrees.

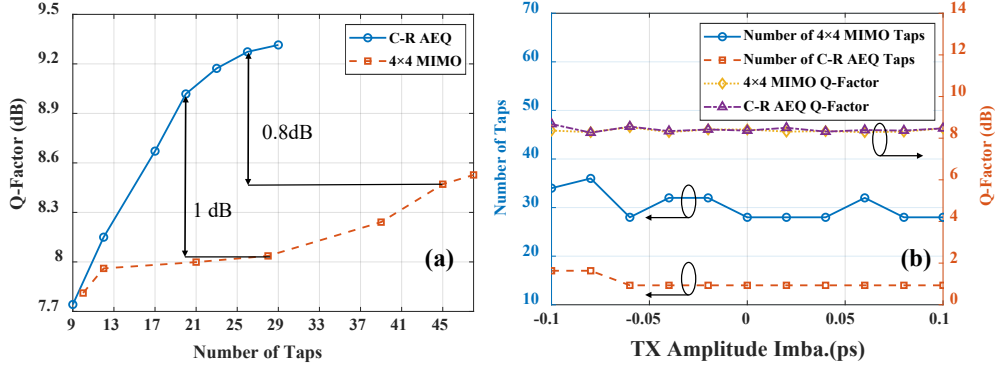


Fig. 18. (a)Q-factor under difference taps(b)The C-R AEQ and 4x4 MIMO required number of taps respectively under the same Q-factor

We also compare the performance of the 4x4 MIMO and C-R AEQ as shown in Fig. 18. Because the 4x4 MIMO only compensates for RX X/Y skew, for fair comparison, in Fig. 18, both TX and RX X/Y pol skew are compensated. In addition, the 4x4 MIMO or C-R AEQ is used for equalizing the same signal data at each comparison. Fig. 18(a) displays the relation between Q-factor and taps. We define the non-butterfly and butterfly filter tap as shown in Eq. 21 and Eq. 22.

$$Tap_{non-butterfly} = \text{ceil}(Tap_{per\ filter} * 2/4) \quad (21)$$

$$Tap_{butterfly} = Tap_{per\ filter} * 4/4 \quad (22)$$

Where $Tap_{per\ filter}$ is the number of taps per filter. In Fig. 18(a), the signal data is at the condition of TX X/Y pol amplitude imbalance -0.1 and TX X/Y pol phase imbalance -10 degrees with zero RX X/Y pol imbalance. The tap of 4x4 MIMO changes from 10 to 48, and C-R AEQ changes from 9 to 29 taps. The CV-MIMO tap is fixed at 6 in C-R AEQ. According to Fig. 18(a), the Q-factor penalty is about 1 dB when comparing the 4x4 MIMO 28 taps and C-R AEQ 17 taps, or comparing the 4x4 MIMO 45 taps and C-R AEQ 27 taps. The reason is that the C-R AEQ equalizes the signal and compensates for the TX amp./pha. imbalance at the same time. In Fig. 18(b), the signal data is at the condition that TX X/Y pol. amplitude imbalance of -0.1 to 0.1, with zero TX X/Y pol. phase imbalance and zero RX X/Y pol. amp./pha. imbalance. Fig. 18(b) shows the number of taps difference between C-R AEQ and 4x4 MIMO under the same Q-factor. On the left Y-axis, the number of taps is plotted as a function of TX amplitude imbalance, for 4x4 MIMO and C-R AEQ. On the right Y-axis, the Q-factors are plotted as a function of TX amplitude imbalance, for 4x4 MIMO and C-R AEQ. According to Fig. 18(b), the C-R AEQ maintains approximately 14 taps(6 taps CV-MIMO+15 taps RV-DD-LMS), with the Q-factor remaining at 8.2 dB. In contrast, even if the TX amp./pha. imbalance is 0, the 4x4 MIMO requires at least 28 taps to achieve the same Q-factor.

4. Complexity

In this part, the complexity of our proposed methods is studied. The complexity of our proposed methods is shown by the number of real multiplications via comparison with other techniques. The signal oversampling rate is 2xsymbol rate.

4.1. CD Compensation Complexity

The pre-chirp filter and FDE are used to compare the complexity. At the signal rate of 36 Gbaud, the block size of the pre-chirp filter is set to 112. According to the data given in reference [22], the pre-chirp filter requires about 14 real multiplications per symbol, whereas the FDE requires about 24 real multiplications per symbol. The complexity is reduced by more than 40%.

4.2. IQ Skew Estimation Complexity

In RX IQ skew estimation complexity area, we select the technique that RX skew estimation based on Godard's phase error detection (Godard's PD) [8] to compare with our proposed RX skew estimation technique in complexity. The complexity calculation includes phase error detection, RX skew estimation, and RX skew compensation. According to reference [8], the Godard's PD requires $20(N_{FFT}/4 + 1)/N_{FFT} + 8\log_2 N_{FFT}$ real multiplications per symbol, where the N_{FFT} is number of point FFT. In general, N_{FFT} is set to 128. Thus, the complexity is 61 real multiplications per symbol. In contrast, the Gardner's PD for skew compensation just requires 18 real multiplications per symbol, and the detail of complexity is that phase error detection, RX skew estimation, and RX skew compensation require 8, 2 and 8 real multiplications per symbol, respectively. The complexity is reduced by more than 70%. The reason is that the XI, XQ, YI, and YQ all need to perform FFTs in Godard's PD, which significantly increases complexity. In rough TX IQ skew estimation complexity area, the TX skew can be adjusted by adjusting the transmitter output delay. Thus, the TX skew compensation has zero complexity.

4.3. AEQ Complexity

The AEQ complexity is calculated by comparing the C-R AEQ and 4×4 MIMO. According to Fig. 18(b), the C-R AEQ requires 6+15 taps with 4×4 MIMO requiring 28 taps when achieve the same Q-factor. According to reference [23], the butterfly filter total requires $4 \times 4 \times N_{tap}$ real multiplications per symbol, and the non-butterfly filter requires $2 \times 4 \times N_{tap}$ real multiplications per symbol, where N_{tap} is the number of taps per filter. Thus, the C-R AEQ requires 216 real multiplications. In contrast, the 4×4 MIMO requires 448 real multiplications. The complexity is reduced by more than 51%.

5. Conclusion

We proposed a low-complexity IQ imbalance compensation architecture. First, the transceiver IQ skew is estimated and compensated for by Gardner's PD and scanning delay. Then, the C-R AEQ consists of a 6-tap CV-MIMO and 15-tap RV-DD-LMS MIMO to equalize the signal and compensate for the TX phase/amplitude imbalance. The simulation and experimental results show that the RX skew estimation error is less than 0.2 ps, and the C-R AEQ can tolerate TX IQ phase/amplitude imbalance. In 100 km 36 Gbaud DP-16QAM signal transmission, the complexity is reduced by about 51%.

References

1. M. Paskov, D. Lavery, and S. J. Savory, "Blind equalization of receiver in-phase/quadrature skew in the presence of nyquist filtering," *IEEE PHOTONICS TECHNOLOGY LETTERS* **25**, 2446–2449 (2013).
2. R. Rios-Mueller, J. Renaudier, and G. Charlet, "Blind receiver skew compensation and estimation for long-haul non-dispersion managed systems using adaptive equalizer," *JOURNAL OF LIGHTWAVE TECHNOLOGY* **33**, 1315–1318 (2015).
3. A. Kawai, M. Nakamura, T. Kobayashi, and Y. Miyamoto, "Digital four-dimensional transceiver iq characterization," *JOURNAL OF LIGHTWAVE TECHNOLOGY* **41**, 1389–1398 (2023).
4. E. P. da Silva and D. Zibar, "Widely linear equalization for iq imbalance and skew compensation in optical coherent receivers," *JOURNAL OF LIGHTWAVE TECHNOLOGY* **34**, 3577–3586 (2016).
5. J. Liang, J. Chai, X. Chen, *et al.*, "Receiver iq imbalance and skew compensation for high order modulation formats by frequency domain 4 x 2 mimo," *JOURNAL OF LIGHTWAVE TECHNOLOGY* **41**, 558–569 (2023).

6. M. Arikawa, M. Sato, and K. Hayashi, "Compensation and monitoring of transmitter and receiver impairments in 10,000-km single-mode fiber transmission by adaptive multi-layer filters with augmented inputs," *OPTICS EXPRESS* **30**, 20333–20359 (2022).
7. N. Stojanovic and X. Changsong, "An efficient method for skew estimation and compensation in coherent receivers," *IEEE PHOTONICS TECHNOLOGY LETTERS* **28**, 489–492 (2016).
8. L. Fang, Y. Zhang, J. Chai, *et al.*, "Anti-singularity clock recovery and rx/tx iq skew compensation scheme," *IEEE PHOTONICS TECHNOLOGY LETTERS* **35**, 1359–1362 (2023).
9. Q. Zhang, Y. Yang, C. Gu, *et al.*, "Multi-dimensional, wide-range, and modulation-format-transparent transceiver imbalance monitoring," *JOURNAL OF LIGHTWAVE TECHNOLOGY* **39**, 2033–2045 (2021).
10. J. Tang, J. Liang, J. Wei, *et al.*, "Non-integer oversampled and robust receiver iq skew monitoring based on modified godard algorithm for short-reach coherent optics," in *2024 IEEE Opto-Electronics and Communications Conference (OECC)*, (2024), pp. 1–3.
11. B. Zou, W. Wang, K. Dong, and F. Li, "Fpga implementation of parallel non-integer oversampling timing recovery with iq skew compensation," in *2025 30th OptoElectronics and Communications Conference (OECC) and 2025 International Conference on Photonics in Switching and Computing (PSC)*, (2025), pp. 1–3.
12. S. Gong, Y. Yang, Q. Xiang, *et al.*, "Hardware efficient and transceiver iq skew-tolerant dsp scheme under baud-rate sampling for short-reach coherent optical interconnects," *JOURNAL OF LIGHTWAVE TECHNOLOGY* **43**, 5645–5652 (2025).
13. S. Gong, Y. Yang, Q. Xiang, *et al.*, "Receiver in-phase and quadrature skew tolerant baud-rate timing recovery scheme for short-reach coherent optical interconnection," *OPTICS LETTERS* **49**, 2845–2848 (2024).
14. J. Tang, H. Chen, S. Cui, *et al.*, "High receiver skew-tolerant and hardware-efficient clock recovery for short-reach coherent transmission," *OPTICS EXPRESS* **30**, 27064–27079 (2022).
15. D. Zibar, J. C. R. F. de Olivera, V. B. Ribeiro, *et al.*, "Experimental investigation and digital compensation of dgd for 112 gb/s pdm-qpsk clock recovery," *OPTICS EXPRESS* **19**, 429–437 (2011).
16. W. Wang, Z. Wu, D. Zou, *et al.*, "Training sequences design for simultaneously transceiver iq skew estimation in coherent systems," *JOURNAL OF LIGHTWAVE TECHNOLOGY* **42**, 5088–5098 (2024).
17. H. Li, Z. Cao, Z. Zhang, *et al.*, "Low-complexity coherent optical transceiver iq imbalances calibration enabled by cross-power spectrum method," *JOURNAL OF LIGHTWAVE TECHNOLOGY* **42**, 8530–8540 (2024).
18. X. Wang, F. Li, M. Yin, *et al.*, "Correlation-based transceiver in-phase/quadrature skew in-field calibration in dual-polarization coherent optical transmission system," *OPTICS EXPRESS* **30**, 22712–22729 (2022).
19. J. Liang, Y. Fan, Z. Tao, *et al.*, "Transceiver imbalances compensation and monitoring by receiver dsp," *JOURNAL OF LIGHTWAVE TECHNOLOGY* **39**, 5397–5404 (2021).
20. M. S. Faruk and K. Kikuchi, "Compensation for in-phase/quadrature imbalance in coherent-receiver front end for optical quadrature amplitude modulation," *IEEE PHOTONICS JOURNAL* **5** (2013).
21. X. Zhou, X. Chen, W. Zhou, *et al.*, "All-digital timing recovery and adaptive equalization for 112 gbit/s polmux-nrz-dqpsk optical coherent receivers," *JOURNAL OF OPTICAL COMMUNICATIONS AND NETWORKING* **2**, 984–990 (2010).
22. A. Felipe and A. L. N. de Souza, "Chirp-filtering for low-complexity chromatic dispersion compensation," *JOURNAL OF LIGHTWAVE TECHNOLOGY* **38**, 2954–2960 (2020).
23. K. Matsuda, R. Matsumoto, and N. Suzuki, "Hardware-efficient adaptive equalization and carrier phase recovery for 100-gb/s/ λ -based coherent wdm-pon systems," *JOURNAL OF LIGHTWAVE TECHNOLOGY* **36**, 1492–1497 (2018).
24. Z. Gong, F. Shi, H. Wang, *et al.*, "Transmitter iq imbalance mitigation using 4×4 real value mimo equalizer based on dd-lms algorithm," in *2023 Opto-Electronics and Communications Conference (OECC)*, (2023), pp. 1–4.